Powder Technology 292 (2016) 46–53

Contents lists available at ScienceDirect

Powder Technology

journal homepage: www.elsevier.com/locate/powtec

Design of a rotor cage with non-radial arc blades for turbo air classifiers

Wenjing Ren [a], Jiaxiang Liu [b], Yuan Yu [a,*]

[a] College of Mechanical and Electrical Engineering, Beijing University of Chemical Technology, Beijing 100029, China
[b] Beijing Key Laboratory of Electrochemical Process and Technology for Materials, Beijing University of Chemical Technology, Beijing 100029, China

ARTICLE INFO

Article history:
Received 4 September 2015
Received in revised form 11 January 2016
Accepted 16 January 2016
Available online 18 January 2016

Keyword:
Turbo air classifier
Rotor cage
Non-radial arc blade
Classification accuracy
Fine powder yield

ABSTRACT

As an important dynamic classifier, turbo air classifiers are widely used in various fields. To improve the classification performance of turbo air classifiers, a novel rotor cage with non-radial arc blades is designed by analyzing the influence of the rotor blade profile and the installed angle on the flow field in a turbo air classifier. Numerical simulations by ANSYS-FLUENT 14.5, as well as material classification experiments, are implemented to verify the new design. Simulation results indicate the significant improvement of flow field distribution in the rotor cage with non-radial arc blades. The incidence angle at the inlet of the rotor cage decreases significantly. Airflow streamlines match the profile of the non-radial arc rotor blade perfectly, and no air vortex is present in the channels of the rotor cage. The material classification experiment results demonstrate that the classification accuracy increases by 10.6%–40.8%, and the fine powder yield increases by 12.5%–40.1%, with an almost changeless cut size. The experimental results agree with the simulation results, thus verifying the feasibility of the modified rotor blades in practice. This design provides a theoretical guidance for the structure improvement of different types of classifiers with a rotor cage.

1. Introduction

Turbo air classifiers are mainstream dynamic classifiers that have simple structures and controllable product granularity. Turbo air classifiers are widely used in various fields, including minerals engineering, fine chemical industry and medicine [1–3]. Given the surge in the demand for ultrafine powder, the requirements of classification performance (e.g., small cut size, high classification accuracy and narrow particle–size distribution) have been increasing gradually. Considering that rotor cages directly affect the interior flow field of turbo air classifiers and classification performance, many researchers have focused on rotor cages. Gao [4] analyzed the effect of rotor cage rotary speed on classification accuracy by using FLUENT software and obtained a reasonable parameter combination for classification. Xing [5] measured and analyzed the vortex swirling between rotor blades by using Particle Image Velocimetry (PIV) technique. They found changes in the regulation of classification efficiency and cut size and obtained optimized operating parameters to obtain the minimum cut size. Ito [6] found that most of the pressure loss in a classifier is produced on the inside of the rotor. To minimize pressure loss and achieve a well-distributed velocity field, the inclined blade was designed.

To improve the flow field distribution in a rotor cage, some researchers made structure improvements [7–10]. Xu [7] designed backward crooked elbow rotor blades and simulated the particle tracks between the rotor blades. Huang [8] simulated and compared the flow field distribution in turbo air classifiers equipped with positively bowed, negatively bowed, and straight guide vanes. He concluded that the inertia rotating vortex and radial velocity fluctuations in rotor cages can be decreased by using positively bowed guide vanes.

Most previous of studies are limited to a given device or configuration and lack a systemic design method. In the present study, the influence of rotor blade configuration on flow field is analyzed thoroughly by referring to the theories of turbo-machinery. A rotor cage with non-radial arc blades is designed to realize a favorable flow field for classification. The rotor blade profile and installed angle are obtained by calculating the airflow velocity and analyzing flow field distribution. ANSYS-FLUENT 14.5 is used to simulate the flow field and compare the rotor cages with non-radial arc blades and straight blades. The experimental data are validated against simulation results to demonstrate that the rotor cage with non-radial arc blades can improve the classification performance of turbo air classifiers.

2. Design of the non-radial arc rotor blade

2.1. Classification principle of the turbo air classifier

The structural scheme of the turbo air classifier used in the present study is shown in Fig. 1-(a). The main geometric dimensions and symbols of the turbo air classifier are as follows: (1) the air inlet is 96 mm in height and 62 mm in width (labeled as a and b, respectively); (2) the outer and inner boundary radii of the rotor cage, R_1 and R_2 are 105 mm and 75 mm, respectively, with 24 blades radially installed and evenly distributed across the circumference of the rotor cage. The

* Corresponding author.
E-mail address: yuyuanjd@263.net (Y. Yu).

http://dx.doi.org/10.1016/j.powtec.2016.01.024
0032-5910/

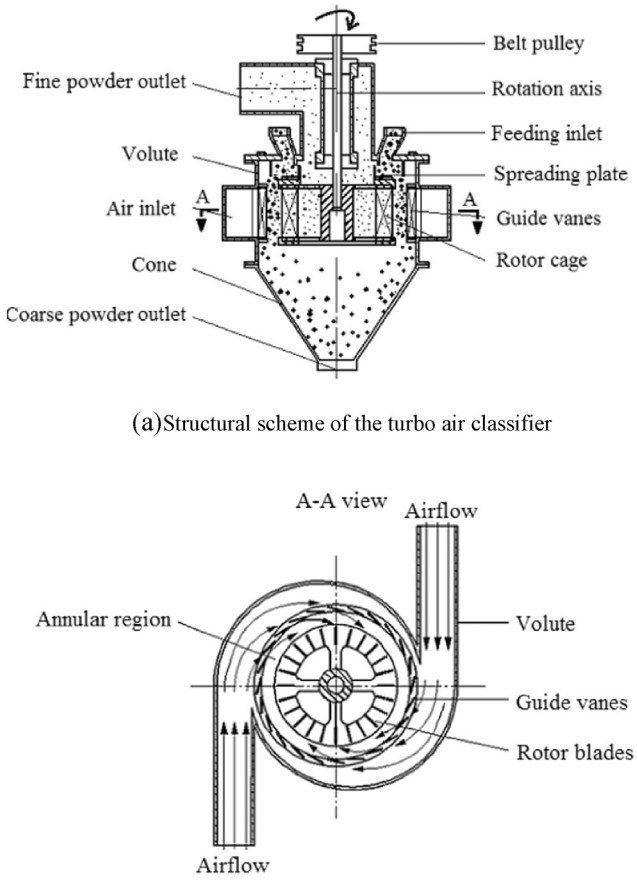

Fig. 1. Schematic of the turbo air classifier.

dimensions of these blades are 30 mm in length, 2 mm in thickness (δ) and 96 mm in height; (3) 24 guide vanes with the same structural dimensions are distributed uniformly along the circumference of a circle with a radius of 136 mm and oriented at an angle of 15° from the tangent at the point on the circle coincident with the vane's centroid.

The rotor cage rotates clockwise and is driven by a belt pulley through the connection of a rotation axis. Under central negative pressure, the airflow enters from two symmetrical air inlets into an annular region through the guide vanes, shown in Fig. 1-(b). The annular region is a cylindrical space between the outer boundary of the rotor cage and the inner boundary of the guide vanes. The powder to be classified enters through the feeding inlet and falls to the spreading plate, which is rapidly rotating together with the rotor cage. The particles are thrown outward into the annular region. Among the many forces acting on the particles in this annular region, the air drag force, centrifugal force and gravity dominate the behavior of the particles [11]. Subject to these forces, small particles with little centrifugal force are drawn through the fine powder outlet, whereas coarse particles with large centrifugal force are thrown out, hit the guide vanes and fall down along the cone, where they eventually fall through the coarse powder outlet.

2.2. Dynamic analysis of a fluid element in the rotor cage

To improve the blade profile according to the flow field characteristics, a fluid element between two blades in the rotor cage is analyzed. On one hand, airflow rotates with the rotor cage. On the other hand, airflow moves inward under the force of the central negative pressure [12]. For a fluid element at any time, its absolute velocity **V** can be divided into relative velocity **W** and transport velocity **U** [13]. A local Cartesian coordinate system consisting of axis **x′** and axis **y′** is set for a fluid element, shown in Fig. 2. The axis **x′** is in the direction of the relative velocity **W**. Axis **y′** is perpendicular to axis **x′**.

The mechanics equilibrium equation in the direction of **y′** can be expressed as Eq. (1) on the basis of the principles of relative motion [14]:

$$P_1 - P_2 = \frac{dP}{dy'} = \rho\left(\omega^2 R_f \cos\beta + \frac{W^2}{R_c} + 2\omega W\right) \tag{1}$$

where,

dP/dy' is the differential incremental pressure along the axis **y′**, and is the pressure difference of P_1 and P_2 acting on the fluid element;
$\Omega^2 R_f \cos\beta$ is the transport acceleration, in which Ω is the rotor cage rotational speed, where β is the relative velocity angle between the relative velocity and the negative direction of transport velocity; R_f is the radius of circle in rotor cage where the fluid element is located;
W^2/R_c is the relative acceleration, where R_c is the curvature radius of streamline where the fluid element is located;
$2\Omega W$ is the Coriolis acceleration;
ρ is the density of air.

The differential form of composite Bernoulli equation in the direction of **y′** is expressed as follows:

$$\frac{dP}{dy'} = \rho\left(U\frac{\partial U}{\partial y'} - W\frac{\partial W}{\partial y'}\right). \tag{2}$$

By substituting $U = \Omega R_f$ and $\cos\beta = dR_f/dy'$ into Eqs. (1) and (2), the linear first-order differential equation of W is derived as follows:

$$\frac{\partial W}{\partial y'} = -2\omega - \frac{W}{R_c}. \tag{3}$$

Eq. (3) indicates that the distribution of relative velocity is only related to the curvature radius of streamline R_c and the rotor cage rotational speed Ω. When the operating parameters are fixed and Ω is constant, R_c becomes the only factor affecting the distribution of relative velocity. The discussions on R_c are made as follows:

1) For straight rotor blades, $R_c = \infty$, the Eq. (3) can be solved as follows:

$$W = -2\omega y' + C_1. \tag{4}$$

2) For the arc rotor blades, the Eq. (3) can be solved as follows:

$$W = e^{\frac{-y'}{R_c}}(C_2 \pm 2\omega R_c) - 2\omega R_c. \tag{5}$$

Using Taylor to expand e^{-y'/R_c}, the Eq. (5) can be substituted with Eq. (6).

$$W = \left(\pm\frac{C_2}{R_c} - 2\omega\right)y' + C_2 \tag{6}$$

where, C_1 and C_2 are positive constants.

Eq. (4) indicates that for the straight rotor blade, the speed variation rate of W is 2 Ω in the direction of axis **y′**. For the arc rotor blade with concave pressure side shown in Fig. 2, the sign ($\pm$) in Eq. (6) is positive ($+$), and the speed variation rate of W is $|-2\omega + C_2/R_c|$. However, for the arc rotor blade with convex pressure side the sign ($\pm$) in Eq. (6) is negative ($-$) and the speed variation rate of W is $|2\omega + C_2/R_c|$. The speed variation rate of W in the direction of axis **y′** is smallest when the

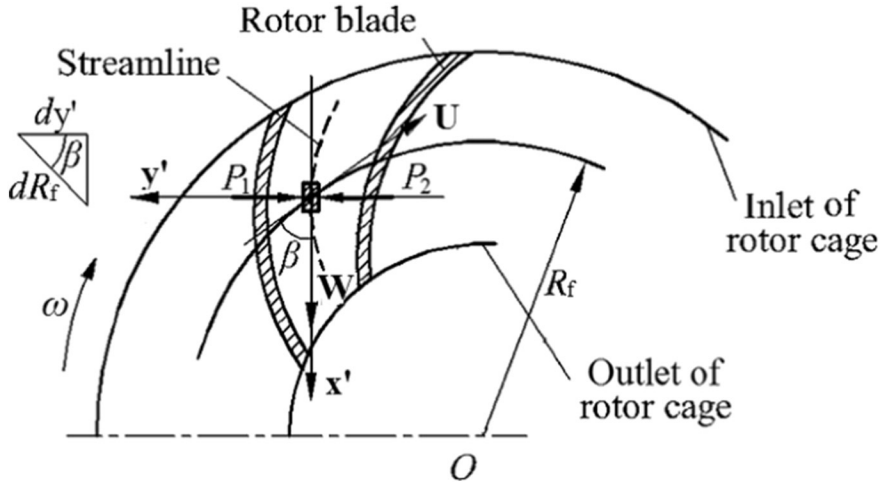

Fig. 2. Dynamic analysis of a fluid element in the channel of the rotor cage.

pressure side of the arc rotor blade is concave. Thus, the flow field in the rotor cage is evenly distributed and the velocity gradient is smaller using the arc rotor blade with concave pressure side than that using the straight rotor blade or arc rotor blade with convex pressure side. Therefore, the arc blade with a concave pressure side is selected in the new design of the rotor cage mentioned in this paper.

2.3. Design of the non-radial arc rotor blade installed angle and profile

According to the arc blade design method in turbo-machinery, the rotor blade installed angle at the inlet and outlet of the rotor cage should be calculated to design the profile of the rotor blade [15,16]. When the incidence angle (i), which is the angle between the incoming airflow and tangential direction of the rotor blade, is not zero or big enough, the airflow will impact the rotor blades with a certain angle [17]. This situation will result in a poor flow field distribution in a rotor cage and will make the particles rebound. Thus, the rotor blade installed angle and profile can be calculated according to the ideal flow field distribution in the rotor cage.

In this paper, a rotor cage rotary speed of 1200 rpm and air inlet velocity of 12 m/s is used as the design condition. By adopting the naming convention of contracting the digits of the air inlet velocity and rotor cage rotary speed, the parameter combination is referred to the 12–1200 case. Two assumptions are made on the basis of the characteristics of a turbo air classifier: (1) the flow field in the turbo air classifier is two-dimensional and rotationally symmetric; (2) the airflow enters the annular region uniformly through the guide vanes (Fig. 3).

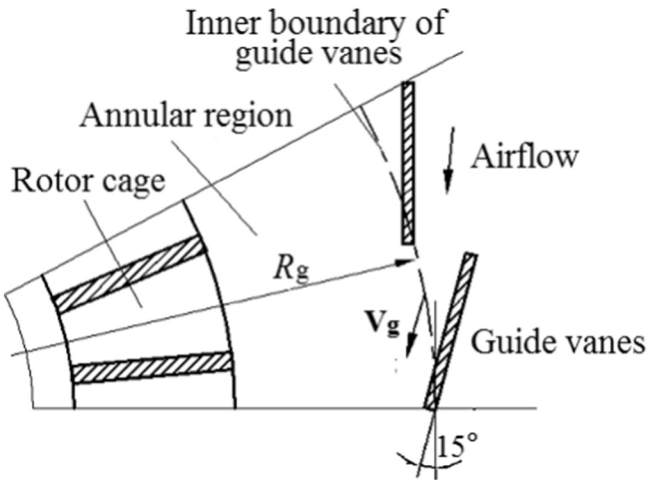

Fig. 3. Schematic of the airflow passing through the guide vanes.

The radius of the inner boundary of the guide vanes R_g is 134 mm. A total of 24 guide vanes are spread along the peripheral direction at the inner boundary of the guide vanes to calculate the airflow velocity at inner boundary of guide vanes.

From continuity equation, the radial velocity V_{gr} at the inner boundary of guide vanes can be obtained:

$$V_{gr} = \frac{Q}{\left(2\pi R_g - \frac{\delta}{\sin\theta} \times n_1\right) \times b} \tag{7}$$

where Q is the total volumetric flow rate of air from the two air inlets and $Q = 2abV_0$; V_0 is the air inlet velocity; n_1 is the number of guide vanes; θ is the guide vane installed angle, which is between the guide vane and tangent of the circle. Furthermore $\theta = 15°$.

According to the second assumption proposed above, the tangential velocity (V_{gt}) can be calculated as follows:

$$V_{gt} = V_{gr}\cot(\theta). \tag{8}$$

Eqs. (7) and (8) can be calculated, and the results are $V_{gr} = 2.3$ m/s, $V_{gt} = 8.5$ m/s.

Airflow meets the angular momentum conservation law when passing through the annular region because no external forces work on the airflow in this region. In equation form, it is expressed as follows:

$$mV_{gt}R_g = mV_{1t}R_1 \tag{9}$$

where m is the mass of the airflow and V_{1t} is the tangential velocity at inlet of the rotor cage.

Thus

$$V_{1t} = \frac{R_g}{R_1}V_{gt}. \tag{10}$$

According to the continuity equation, the radial velocity at the inlet of the rotor cage can be written as follows:

$$V_{1r} = \frac{Q}{\left(2\pi R_1 - \frac{\delta}{\sin\alpha_1} \times n_2\right) \times b} \tag{11}$$

where α_1 is the inlet installed angle, which is the angle between the

tangent of the rotor blade and the tangent of the circle at the inlet of the rotor cage; n_2 is the number of rotor blades.

The magnitude of absolute velocity at inlet of rotor cage is expressed as follows:

$$V_1 = \sqrt{{V_{1r}}^2 + {V_{1t}}^2}. \tag{12}$$

The absolute velocity angle (γ), between absolute velocity and circumferential direction is expressed as follows:

$$\gamma = \mathrm{arctg}\left(\frac{V_{1r}}{V_{1t}}\right). \tag{13}$$

The transport velocity U_1 is equal to the circumferential velocity at the inlet of the rotor cage, which can be written as follows:

$$U_1 = \frac{2\pi R_1 N \times 10^{-3}}{60} \tag{14}$$

where, N is the rotor cage rotary speed.

The relative velocity at the inlet of the rotor cage can be calculated according the inlet velocity triangle shown in Fig. 4. β_1 is the relative velocity angle at the inlet of the rotor cage.

According to the cosine theorem, the magnitude of the relative velocity at the inlet of the rotor cage is written as follows:

$$W_1 = \sqrt{{U_1}^2 + {V_1}^2 - 2U_1V_1\cos\gamma}. \tag{15}$$

The relative velocity angle is expressed as follows:

$$\beta_1 = \cos^{-1}\left(\frac{{U_1}^2 + {W_1}^2 - {V_1}^2}{2U_1W_1}\right). \tag{16}$$

For the traditional rotor cage, $\alpha_1 = 90°$. Given that α_1 is not equal to β_1, a big incidence angle will be produced at the inlet of the rotor cage. A large incidence angle will be harmful to the classification. Thus, the relative velocity angle should be equal to the rotor blade installed angle ($\alpha_1 = \beta_1$) to avoid the bad influence caused by the incidence angle. The relative velocity magnitude and relative velocity angle can be calculated using Eqs. (11)–(16) with the interpolation method. The results are $W_1 = 3.4$ m/s, $\alpha_1 = \beta_1 = 45.4°$. Given that α_1 is equal to β_1, the incidence angle ($i = \alpha_1 - \beta_1$) is zero.

Airflow passes though the rotor cage along the rotor blade profile with no changes on the mass of airflow. Thus, Eq. (17) can be obtained according to the continuity equation:

$$2\pi R_1 W_1 \sin\alpha_1 \approx 2\pi R_2 W_2 \sin\alpha_2 \tag{17}$$

where W_2 and α_2 are the relative velocity and installed angle at the outlet of the rotor cage. A smaller change of relative velocity in the rotor cage leads to the lower incidence of air vortex in the channels of the rotor cage [18]. Therefore, the relative velocity in the rotor cage is expected to be constant. The relative velocity angle at the outlet of the rotor cage can be estimated as follows after inserting the equation $W_1 = W_2$:

$$\alpha_2 \approx \sin^{-1}\left[\frac{R_1}{R_2}\sin\alpha_1\right]. \tag{18}$$

The calculated result of Eq. (18) is $\alpha_2 = 85.4°$. The inlet and outlet installed angles α_1 and α_2 are rounded as 45° and 85°. With α_1 and α_2, the profile of the non-radial arc rotor blade can be plotted as shown in Fig. 5. In this figure, O and M are the centers of the rotor cage and arc blade profile, respectively; R_b is the radius of the blade profile.

By applying the cosine theorem in the triangle AOM and triangle BOM, the following equations can be obtained:

$$OM^2 = R_1^2 + R_b^2 - 2R_1R_b\cos\alpha_1 \tag{19}$$

$$OM^2 = R_2^2 + R_b^2 - 2R_2R_b\cos\alpha_2. \tag{20}$$

The radius R_b and length of OM can be calculated using Eqs. (19) and (20); the results are 40 mm and 82 mm, respectively. Given that the position and radius of the arc rotor blade profile have been confirmed, the design of the non-radial arc rotor blade is finished.

3. Numerical simulation and comparison of rotor cages with straight and non-radial arc blades

3.1. Model description

In this numerical simulation, the geometry and grid were created using the preprocessor GAMBIT 2.4.6. The CFD simulations were performed using FLUENT-ANSYS 14.5. The model was designed to describe the main classification domains, including three regions: the volute, rotor cage and center (Fig. 6-(a)). The structured Hex & Wedge grids and the Cooper algorithm were applied to these domains. The geometry

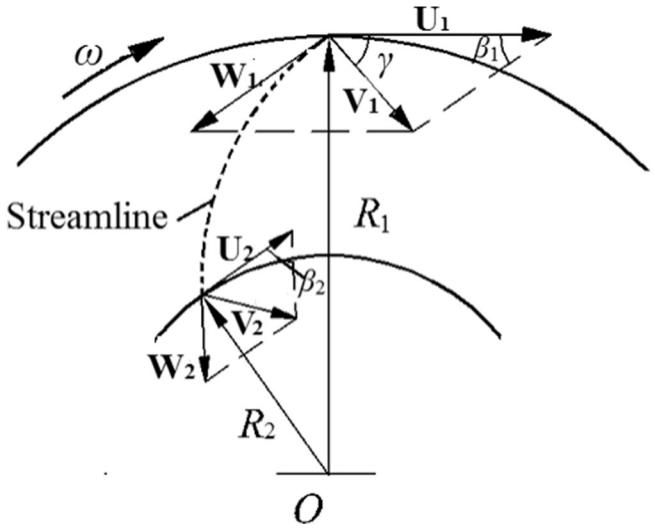

Fig. 4. Velocity triangles at the inlet and outlet of the rotor cage.

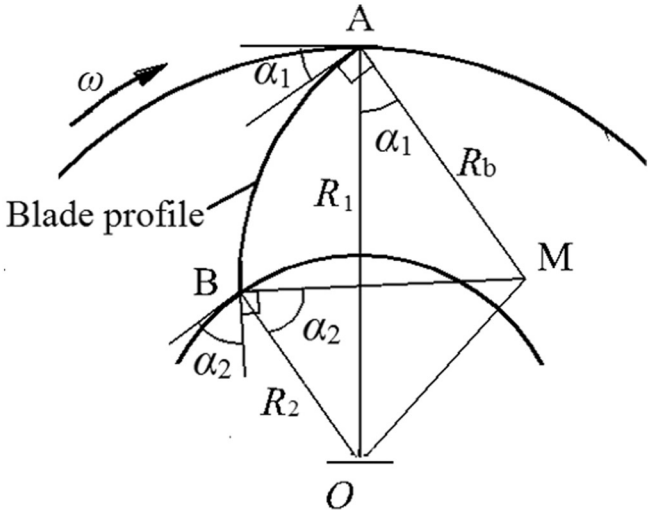

Fig. 5. Schematic of the plotting rotor blade profile.

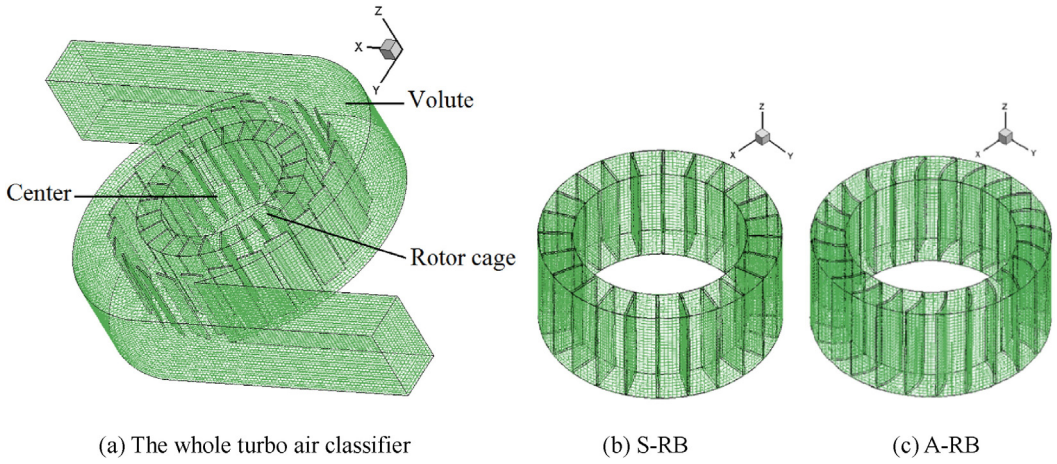

Fig. 6. Meshes of the turbo air classifier.

model of the turbo air classifier with non-radial arc rotor blades (labeled as A-RB) and straight rotor blades (labeled as S-RB) were created, respectively (Fig. 6-(b) and (c)).

Three-dimensional Reynolds–averaged Navier–Stokes equations, along with the RNG *k-ε* turbulence model, are adopted to describe the airflow, suitable for the simulation of turbulent flow in the high strain rate and curvature of streamline [19]. On the basis of the proposal of Launder and Spalding, no-slip boundary conditions are used for wall boundaries, and standard wall-function conditions are used at the near-wall flow regions [20]. The coupling of pressure and velocity is completed using SIMPLEC algorithm in terms of calculation accuracy and time. An air inlet velocity of 12 m/s is prescribed, and a rotor cage rotary speed of 1200 rpm is set.

3.2. Analyses of the numerical simulation results

The velocity distributions at an XOY-plane with Z = 50 mm for a rotor cage with different types of blades are discussed as follows. Given that the turbo air classifier is axisymmetric, half of the horizontal section of the model is discussed.

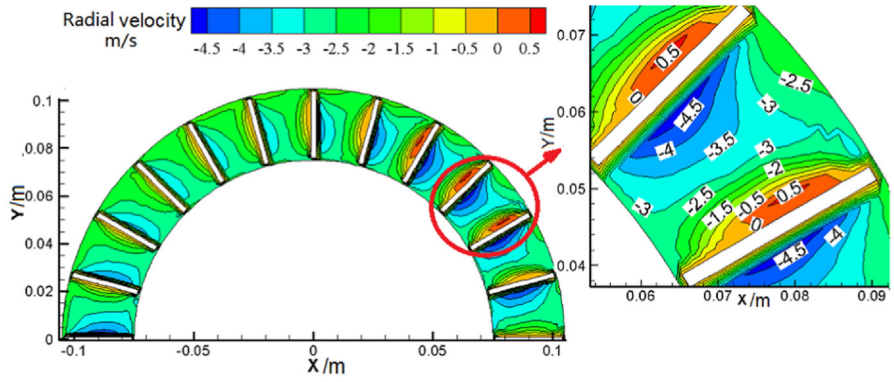

(a) S-RB rotor cage

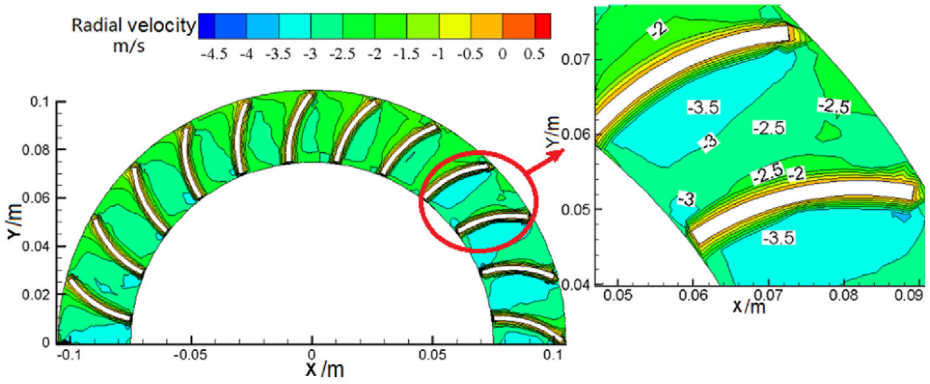

(b) A-RB rotor cage

Fig. 7. Comparison of the radial velocity distributions in the S-RB and A-RB rotor cages.

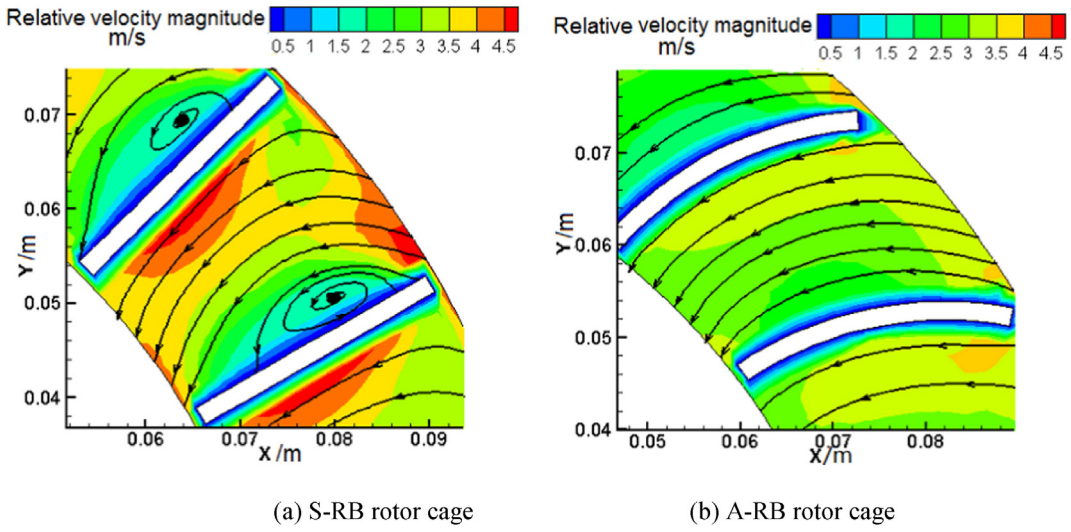

Fig. 8. Relative velocity distribution contours and streamlines in the channel of S-RB and A-RB rotor cages. (a) S-RB rotor cage. (b) A-RB rotor cage.

The radial velocity distributions in the channels of the S-RB and A-RB rotor cages are shown in Fig. 7. Different colors represent different velocity values, and a negative sign (−) indicates that the radial velocity point towards the center of the rotor cage. For the S-RB rotor cage, the flow field is not well-distributed (Fig. 7-(a)). The radial velocities in the channels of the S-RB rotor cage change from −4.5 m/s to 0.5 m/s. The large radial velocity gradient will cause the back-mixing of both coarse and fine particles [21,22]. Some coarse particles are probably dragged into the rotor cage by airflow with the action of the large radial velocity (−4.5 m/s) near the pressure side of the rotor blade. These coarse particles are then collected as fine powder. However, fine particles that are dragged into the channels of the rotor cage will probably be returned to the annular region and mixed with the coarse powder by airflow with the positive radial velocity (0.5 m/s) near the suction side of the rotor blade. As a result, the classification accuracy will decrease. For the A-RB rotor cage, the flow field is fairly well-distributed (Fig. 7-(b)). The radial velocities in channels of the A-RB rotor cage change from −3.5 m/s to −2 m/s. As a result, the probability of the coarse and fine particles back-mixing into each other is decreased.

Fig. 8 is the relative velocity distribution contours and streamlines in the channels of the S-RB and A-RB rotor cages. Different colors represent the different values of relative velocity. The curves with arrows represent the airflow streamlines. In Fig. 8-(a), relative velocities in S-RB rotor cage range from 0.5 m/s to 4.5 m/s. The air streamlines have a sharp deflection at the inlet of the rotor cage, thus indicating a big incidence angle exists between the rotor blade and incoming airflow. Air vortexes are clearly observed near the suction side of the blades. By contrast, the relative velocity distribution in the A-RB rotor cage is greatly improved. The relative velocity gradient in the channels of the rotor cage is decreased (between 2 and 3.5 m/s) and the flow field becomes well-distributed. The airflow streamlines are approximately in accordance with the rotor blade profiles. The deflection of the streamlines at the inlet of the rotor cage, as well as the air vortexes in the channels of rotor cage, disappears.

Thus, the flow field characteristics in the A-RB rotor cage are more favorable for classification than that in the S-RB rotor cage.

4. Experiment verification

To verify the simulation results, calcium carbonate powder classification experiments were conducted with different air inlet velocities and rotor cage rotary speeds, including 12–1200, 10–1200, 8–1200 and 12–1000. Raw material is fed by a screw feeder at a feed rate of 120 kg/h. The particle-size differential distribution of the calcium carbonate powder used in the experiments is listed in Table 1. The S-RB and A-RB rotor cages are used for comparison. For every experiment, the mass of coarse powder, fine powder and raw material are weighed by a platform scale. The samples are then collected from the coarse powder, fine powder and raw material using Sieving Riffler. The particle-size differential distributions for these samples can be obtained using an Easysizer20 Laser Particles Size Analyzer. The calibration of the scale is 0.05 kg/100 kg, and the labelled repeatability error of the size analyzer is less than 3%.

The cut size and classification efficiency can be calculated by analyzing the Tromp curve [23]. The cut size d_{50} refers to the particle size at the point where the partial classification efficiency is 50%. The gradient of the Tromp curve reflects the classification accuracy K and is expressed as $K = d_{25}/d_{75}$, where d_{25} refers to the particle size at the point where the partial classification efficiency is 25% and d_{75} refers to the particle size at the point where the partial classification efficiency is 75%. The steepness of the curve also increases, thus indicating that K is closer to one. Under ideal conditions, $K = 1$. The fine powder yield η is calculated by dividing the mass of the collected fine powder by the mass of the raw material. The results using A-RB and S-RB rotor cage are reported in Table 2. The results show that the classification accuracy K increases by 10.6% — 40.8% and that the fine powder yield η increases by 12.5% — 40.1% using the A-RB rotor cage compared with the S-RB rotor cage, with almost changeless cut size. Under the design condition of the 12–1200 case, the classification accuracy and fine powder yield are increased by 40.8% and 12.5%, respectively.

The particle-size differential distribution of classification results with different cases is shown in Fig. 9. In Fig. 9-(a), for the collected fine powder, the particles with differential frequencies larger than 1.25% range from 4 μm to 46 μm by using the A-RB rotor cage. However,

Table 1
Particle size differential distribution of calcium carbonate.

Particle size (μm)	<1.8	1.8–6.4	6.4–16.6	16.6–25.4	25.4–38.8	38.8–53.5	53.5–73.6	>73.6
Differential distribution (%)	2.78	8.37	15.30	22.23	25.19	17.72	7.98	0.43

Table 2
Comparison of d_{50}, K and η of the S-RB and A-RB rotor cages.

Air inlet velocity (m/s)	Rotor cage rotary speed (rpm)	d_{50} (μm)		K (%)		η (%)	
		S-RB	A-RB	S-RB	A-RB	S-RB	A-RB
12	1200	26.0	26.8	43.9	61.8	40.0	45.0
10	1200	22.4	24.2	35.4	44.5	25.0	35.0
8	1200	19.6	21.4	30.0	38.6	18.1	21.3
12	1000	28.6	29.0	42.3	46.8	43.8	50.0

particles with differential frequencies larger than 1.25% range from 4 μm to 58 μm by using S-RB rotor cage. Thus, the particle-size distribution of the collected fine powder by using A-RB rotor cage is narrower than that using S-RB rotor cage. The amount of coarse particles in fine powder by using the A-RB rotor cage is less than that by using S-RB rotor cage. Taking 40 μm particles in Fig. 9-(a) as an example, the differential frequency in fine (A-RB) is 2.3%; however, the differential frequency in fine (S-RB) is 4.7%. This result indicates that less coarse particles mix into the fine powder, particularly the coarse particles in 28–70 μm diameters in the case of the A-RB rotor cage. For the collected coarse powder, less fine particles from the 1–22 μm mix into the coarse powder. Furthermore, the above improvements are remarkable when the operation condition is close to the design condition of the 12–1200 case. For example, for the 8–1200 case in Fig. 9-(c), the particle-size differential distribution of the collected fine powder is almost identical by using the A-RB rotor cage and S-RB rotor cage.

The experimental results indicate that the A-RB rotor cage can increase the classification accuracy and fine powder yield of the turbo air classifier and obtain the fine powder with narrow particle-size distribution. The classification experimental results are in good agreement with the numerical simulations.

5. Conclusions

This study proposes a systemic common design method of rotor blades for classifiers and designs a rotor cage with non-radial arc blade on the basis of the analysis of ideal flow field characteristics in turbo air classifiers. The material classification experiments results agree with the numerical simulations, verifying the practicability of this new design. This research provides a theoretical guidance for the structure optimization of other types of classifier. Two important conclusions can be obtained as follows:

(1) An arc rotor blade with a concave pressure side is selected as the rotor blade to decrease the velocity gradient and probability of air vortexes in the rotor cage. When the relative velocity angle is equal to the rotor blade installed angle, the incidence angle between the airflow and rotor blade is zero. This situation avoids the impact of airflow and particles on the rotor blades. The well-distributed flow field in the rotor cage is improved greatly. Simulation results verify the feasibility of the new design.
(2) The classification experiments show the following: compared to the rotor cage with straight blades, the classification accuracy of a rotor cage with non-radial arc blades is increased by 10.6%–40.8%; the fine powder yield is increased by 12.5%–40.1% with different operating parameters. Moreover, a fine powder with narrow particle-size distribution can be obtained by using a rotor cage with non-radial arc blades.

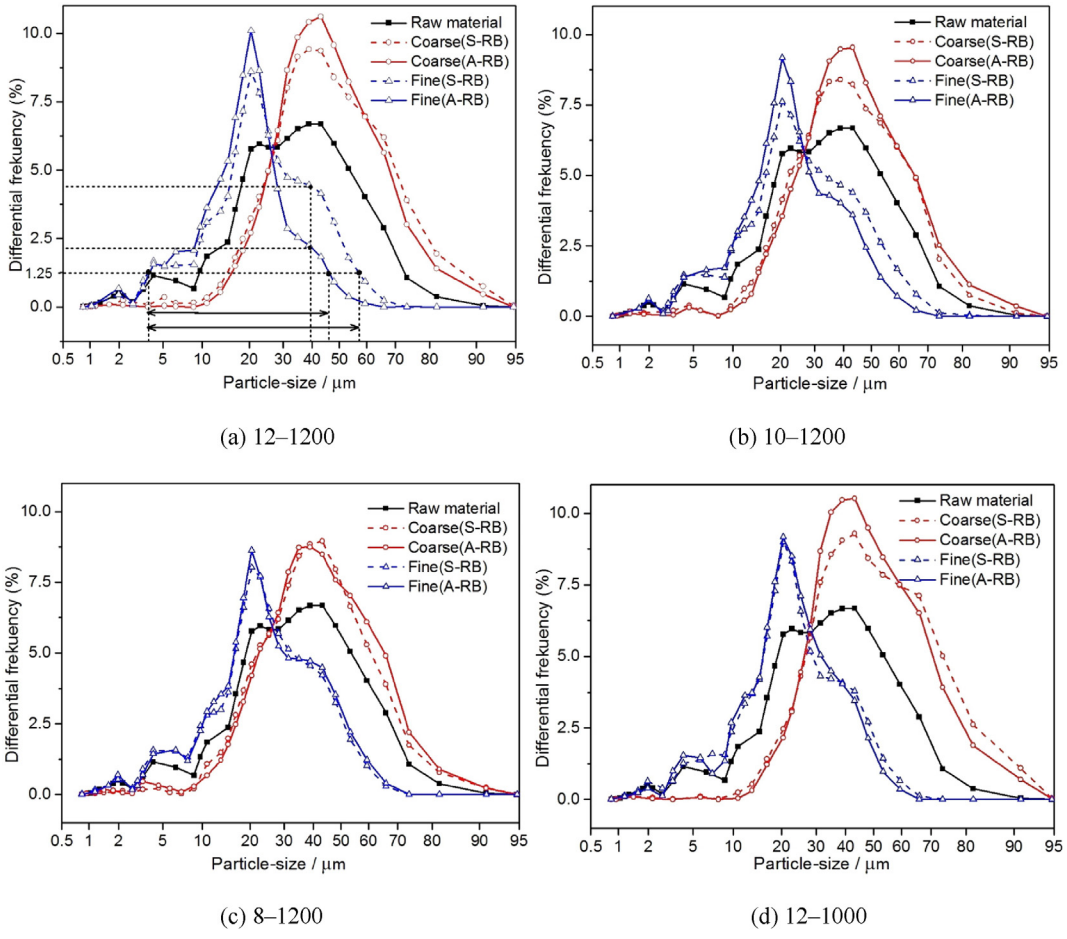

Fig. 9. Particle-size distributions of the classification results with different operating parameters.

Nomenclature

a	height of the air inlet (mm)
b	width of the air inlet (mm)
C_1, C_2	positive constants
d_{50}	cut size of classification (μm)
K	classification accuracy (%)
m	mass of airflow (kg/s)
N	rotor cage rotary speed (rpm)
n_1	number of guide vanes
n_2	number of rotor blades
P	pressure acted on fluid element (Pa)
Q	total volumetric flow rate of air (cm^3/s)
R_b	radius of rotor blade profile (mm)
R_c	curvature radius of streamline (m)
R_f	radius of fluid element located section (m)
R_i	radius of section in rotor cage (mm)
U_i	transport velocity (m/s)
V_0	air inlet velocity (m/s)
V_{ij}	absolutely velocity (m/s)
W_i	relative velocity (m/s)
α_i	rotor blade installed angle (°)
β_i	relative velocity angle (°)
γ	absolute velocity angle (°)
i	incidence angle (°)
θ	guide vane installed angle (°)
ω	rotor cage rotational speed (rad/s)
ρ	density of air (kg/m^3)
δ	thickness of rotor blade or guide vane (mm)
η	fine powder yield (%)

Subscript

i = null, 1, 2, g the position of fluid element located, the inlet of rotor cage, the outlet of rotor cage, the inner boundary of guide vanes.

j = null, r, t the magnitude, tangential, radial value of velocity.

Acknowledgement

This project is supported financially by the National Natural Science Foundation of China (No. 51204009).

References

[1] M. Shapiro, V. Galperin, Air classification of solid particles: a review, Chem. Eng. Process. Process Intensif. 44 (2005) 279–285.
[2] Y. Yu, J. Liu, K. Zhang, Establishment of a prediction model for the cut size of turbo air classifiers, Powder Technol. 254 (2014) 274–280.
[3] Y. Yu, J. Liu, Classification performance comprehensive evaluation of an air classifier based on fuzzy analytic hierarchy process, Mater. Werkst. 44 (2013) 897–902.
[4] L. Gao, Y. Yu, J. Liu, Effect of rotor cage rotary speed on classification accuracy in turbo air classifier, CIESC J. 63 (2012) 1056–1062.
[5] W. Xing, Y. Wang, Y. Zhang, Y. Yamane, M. Saga, J. Lu, H. Zhang, Y. Jin, Experimental study on velocity field between two adjacent blades and gas–solid separation of turbo air classifier, Powder Technol. 286 (2015) 240–245.
[6] M. Ito, Y. Miyabe, F. Kawano, The forms of the rotor blades system and pressure loss within a cage-type centrifugal air classifier, J. Soc. Powder Technol. 33 (1996) 253–261.
[7] N. Xu, G. Li, Z. Huang, Numerical simulation of particle motion in turbo classifier, China Particuology 3 (2005) 275–278.
[8] Q. Huang, J. Liu, Y. Yu, Turbo air classifier guide vane improvement and inner flow field numerical simulation, Powder Technol. 226 (2012) 10–15.
[9] R. Liu, J. Liu, Y. Yu, Effects of axial inclined guide vanes on a turbo air classifier, Powder Technol. 280 (2015) 1–9.
[10] C. Eswaraiah, S.I. Angadi, B.K. Mishra, Mechanism of particle separation and analysis of fish-hook phenomenon in a circulating air classifier, Powder Technol. 218 (2012) 57–63.
[11] L. Guo, J. Liu, S. Liu, J. Wang, Velocity measurements and flow field characteristic analyses in a turbo air classifier, Powder Technol. 178 (2007) 10–16.
[12] J. Liu, J. Xia, T. He, Classifying function regions in a turbo air classifier, J. Beijing Univ. Chem. Technol. 29 (2002) 50–53.
[13] C. Scheit, B. Karic, S. Becker, Effect of blade wrap angle on efficiency and noise of small radial fan impellers—a computational and experimental study, J. Sound Vib. 331 (2012) 996–1010.
[14] L. An, Y. Lv, Pump & Fan, China Electric Power Press, Beijing, 2008.
[15] W. Li, Effects of viscosity on turbine mode performance and flow of a low specific speed centrifugal pump, Appl. Math. Model. 40 (2016) 904–926.
[16] S. Lin, C. Huang, An integrated experimental and numerical study of forward-curved centrifugal fan, Exp. Thermal Fluid Sci. 26 (2002) 421–434.
[17] D. Pan, Discussion of the best incidence angle in centrifugal fan, Compressor Blower Fan Technol. 1 (2009) 13–15.
[18] Z. Tie, Z. Liu, The Design and Application of Fluid Machinery Principle, China Electric Power Press, Beijing, 2009.
[19] R. Guta, M.D. Kaulaskar, V. Kumar, R. Sripriya, B.C. Meikap, S. Chakraborty, Studies on the understanding mechanism of air core and vortex formation in a hydrocyclone, Chem. Eng. J. 144 (2008) 153–166.
[20] Y. Yu, Fluent Introductory and Advanced Tutorial, Beijing Institute of Technology Press, China, 2010.
[21] L. Gao, Y. Yu, J. Liu, Study on the cut size of a turbo air classifer, Powder Technol. 237 (2013) 520–528.
[22] H. Morimoto, T. Shakouchi, Classification of ultra fine powder by a new pneumatic type classifier, Powder Technol. 131 (2003) 71–79.
[23] Y. Kosaki, T. Hiral, Y. Yamanaka, K. Takeshima, Investigation on dust collection and particle classification performance of cyclones by airflow control for design of cyclones, Powder Technol. 277 (2015) 22–35.